Control of surface roughness by varying the temperature while a thin film is deposited

Edwin Edgar Mozo Luis,[*] Thiago A. de Assis,[†] and Fábio D. A. Aarão Reis[‡]
Instituto de Física, Universidade Federal Fluminense, Avenida Litorânea s/n, 24210-340 Niterói, RJ, Brazil

(Received 30 July 2025; revised 22 October 2025; accepted 7 April 2026; published 27 April 2026)

In thin film deposition from vapor at constant substrate temperature, the surface roughness may reach large values as the thickness increases or as multilayer islands form in the initial growth stages. Here, we use kinetic Monte Carlo (KMC) simulations of four models of thin film deposition with dynamically changing substrate temperature to search for conditions to reduce the roughness of a variety of surface morphologies of applied relevance. At constant temperature, these models lead to: (1) kinetic roughening of the film surfaces; (2) growth of uncorrelated mounds whose widths increase with the temperature; (3) mound coarsening with selection of slopes that increase with the temperature; and (4) growth of multilayer islands on a foreign substrate and their coalescence to form a continuous film. In all simulations, we consider linearly increasing and linearly decreasing temperatures. With models 2 and 4, time-increasing temperature during the deposition produces final surfaces with smaller roughness than those produced by deposition at any temperature in the same range. This occurs because narrow mounds or islands nucleate at the lowest temperatures and, as the temperature increases, the larger diffusion lengths of the adsorbed species lead to rapid filling of the gaps or valleys, allowing faster coalescence of mounds and islands, and consequent surface smoothening. This physical interpretation shows that deposition in time-increasing temperature may be a route for producing smoother films when high densities of islands or mounds are formed at the lowest temperatures (which is the common feature of models 2 and 4). In the simulations of models 1 and 3, as well as with time-decreasing temperature in all models, a similar effect is not observed, but nontrivial evolutions of the roughness (e.g., nonmonotonic variations) may be found, which significantly differ from the growth modes observed in constant temperature deposition. A method to interpolate the roughness evolution of KMC simulations at constant temperatures is also proposed, but for all models, we show that the growth history in time-varying temperature cannot be quantitatively predicted by interpolation of data obtained in constant temperature growth.

DOI: 10.1103/2hd9-tfbb

I. INTRODUCTION

The deposition of thin solid films is essential for the fabrication of several electronic devices, magnetic storage media, and energy devices, among other applications [1]. The advance of these technologies frequently requires the decrease in the film thickness; for instance, ∼15 nm C_{60} layers were recently shown to optimize the performance of perovskite solar cells [2], and 1 nm layers grant the best performance of field-effect transistors based on a reduced graphene oxide electrode [3]. The film uniformity is also necessary to warrant the same physical and chemical behavior in large areas. For several applications, the film uniformity has to be controlled during the growth because further smoothening by high-temperature annealing may damage parts of the devices. This is a motivation for developing strategies to grow films with low roughness.

When thin films are deposited from vapor sources, the relaxation of the adsorbed material by diffusion is expected to be the main mechanism controlling the morphologies. The relaxation favors the formation of low-energy configurations, which usually correspond to smooth surfaces at large length scales. However, even with slow deposition and at high temperatures, the desired layer-by-layer growth may not be obtained if the relaxation time is too large compared to the deposition time, i.e., in conditions far from thermodynamic equilibrium. This is the case, for instance, of mound formation with slope selection in homoepitaxial deposition of metals such as copper and iron [4–6], which is explained by growth models with thermally activated diffusion of the adsorbed atoms (adatoms) [4,7–10]. In film deposition on substrates of different materials, other growth modes (i.e., other types of morphological evolution) are observed. In recent years, several studies showed the growth of high islands followed by their coalescence and continuous film formation, such as sputter deposition of Ag, Au, and Pd films [11], thermal evaporation of perovskite films [12,13], hot wall CdTe deposition [14], and evaporation of organic films [15,16]. The same features were qualitatively shown in recent kinetic Monte Carlo (KMC) simulations of deposition models with layer-dependent diffusion coefficients [14,16–18]. In the initial stages of heteroepitaxy, strain also has nontrivial effects on the morphology [1]. When the film thicknesses are large, their surfaces may also show kinetic roughening, in which the roughness and the lateral correlations scale as power laws of time and distance as predicted by stochastic growth equations [19,20].

[*]Contact author: mozo2920@gmail.com
[†]Contact author: thiagoaa@id.uff.br
[‡]Contact author: fdaar@protonmail.com

The effects of the temperature on the above-mentioned growth modes are known, but in all studies, the temperature remained constant during the deposition. A relevant question is whether a dynamic temperature control can be an alternative route for the fabrication of smooth films because that control can increase or decrease the surface diffusion lengths of the adsorbed species while the film grows. Effects of time-varying temperature were formerly studied in a simple deposition model in which only isolated atoms on terraces are mobile and which exhibits kinetic roughening if the temperature is kept constant [21]. The evolution of the surface roughness could be approximated by assuming that the film evolved through a sequence of states representative of deposition in each intermediate temperature and thickness [21]. In other works, changes in the parameters of models with kinetic roughening were performed during the growth (sudden and continuous changes were considered) [22–26]. They led to a variety of effects on the interface roughness and, in some cases, the applied changes could be related to temperature changes [24,25]. However, these models do not describe other experimentally relevant growth modes, i.e., other types of morphological evolution such as mound formation and multilayer island growth [8,10]. Moreover, to the best of our knowledge, no experimental work has shown the effect of temperature variation during film growth.

Here, we study four models of film deposition with thermally activated diffusion of the adsorbed species, considering dynamically evolving (increasing or decreasing) temperatures during the deposition. These models provide several morphologies that can be experimentally observed at constant temperature. We begin with the Clarke-Vvedensky (CV) model [10,27] without Ehrlich-Schwoebel (ES) barriers for crossing step edges [28,29], which shows kinetic roughening [30,31]. We further consider two deposition models with ES barriers which lead to nucleation and growth of correlated or uncorrelated mounds [4,6,7,32–42]. Finally, we study a model that represents deposition of a film on a foreign substrate where film-substrate interactions are weaker than film-film interactions [14]; these mechanisms lead to nucleation and growth of islands that eventually coalesce to form a continuous film, as observed in recent experiments [12,14–16]. We perform KMC simulations of these four models at constant temperature and with temperature variations of less than 1 K during the deposition of each atomic or molecular layer.

In some conditions, we show that the dynamic increase of the temperature smoothens the film surface in comparison with the growth when the initial or the final temperature is kept constant. This is the case, e.g., when there is multilayer island growth in the initial stages of the deposition on foreign substrates. The smoothening is a consequence of the high densities of islands or mounds produced at early times (at the lowest temperatures) and of the rapid filling of the valleys or gaps due to the increased surface mobility at the highest temperatures. In parallel, we develop a method to interpolate the film roughness evolution obtained in KMC simulations at constant temperatures and show that it fails to reproduce the roughness evolution in time-varying temperature in several cases, which contrasts with previous results for a simpler growth model [21]. For this reason, the results obtained here in each model have to be physically interpreted in terms of their particular microscopic dynamics.

II. MODELS AND METHODS

A. Deposition models

All films are grown with a simple cubic (SC) lattice structure to simplify the simulations, and all measured lengths are in units of the lattice constant. The flat substrate is located at $z = 0$, and the substrate atoms are immobile. Each adsorbed atom or molecule occupies a single site at $z \geqslant 1$; for simplicity, an adsorbed atom or molecule is hereafter referred to as an adatom. Solid-on-solid (SOS) conditions are considered, so that the deposits have no pores, and periodic boundaries are considered in the x and y directions. The adatoms with the same (x, y) position form a column of the deposit, and the height variable $h(x, y)$ is the z coordinate of the topmost adatom of that column.

The atomic (or molecular) flux has a rate of F atoms per column per unit time (t). The incidence of each new atom is implemented by randomly choosing an incidence column (x, y) and by its adsorption at the top of that column. Here, we study four models of adatom relaxation which represent homoepitaxial growth (models 1, 2, and 3) and growth on foreign substrates (model 4). In all models, the relaxation is restricted to the adatoms currently located at the top of the columns; the adatoms below the column tops are immobile, but they become mobile if the adatoms above them hop to other columns. Desorption is neglected in all cases.

Model 1. Clarke-Vvedensky (CV) model [27] without ES barriers.

The CV model provides a good approximation for the initial stages of metal homoepitaxy [10], such as Fe/Fe(001) [43] and Ag/Ag(001) [44]. The absence of ES barriers generally prevents the application of this model to multilayers, but it has shown interest for investigations of kinetic roughening [45]: at constant temperature, the surface roughness evolves as predicted by the Villain-Lai-Das Sarma (VLDS) stochastic growth equation [30,31].

The relaxation in the CV model is represented by thermally activated adatom hops to the tops of the neighboring columns $[(x \pm 1, y)$ or $(x, y \pm 1)]$. When an adatom attempts to hop, the target direction is randomly chosen among the four neighboring columns. The hopping rate (number of hops per unit of time) of an adatom with N lateral nearest neighbors (NNs) is

$$D = D_0 \epsilon^N, \tag{1}$$

where

$$D_0 = \nu \exp\left[-E_A/(k_B T)\right], \tag{2}$$

is the hopping rate on terraces (no lateral NN), and

$$\epsilon \equiv \exp\left[-E_B/(k_B T)\right]. \tag{3}$$

In Eqs. (1) and (3), ν is a frequency, $E_A > 0$ and $E_B > 0$ are activation energies, k_B is the Boltzmann constant, and T is the substrate temperature.

Figure 1(a) illustrates the incidence of an atom and three particle hops. Observe that the hopping rates of model 1 do not depend on the positions z of the adatom at the current position and at the target column.

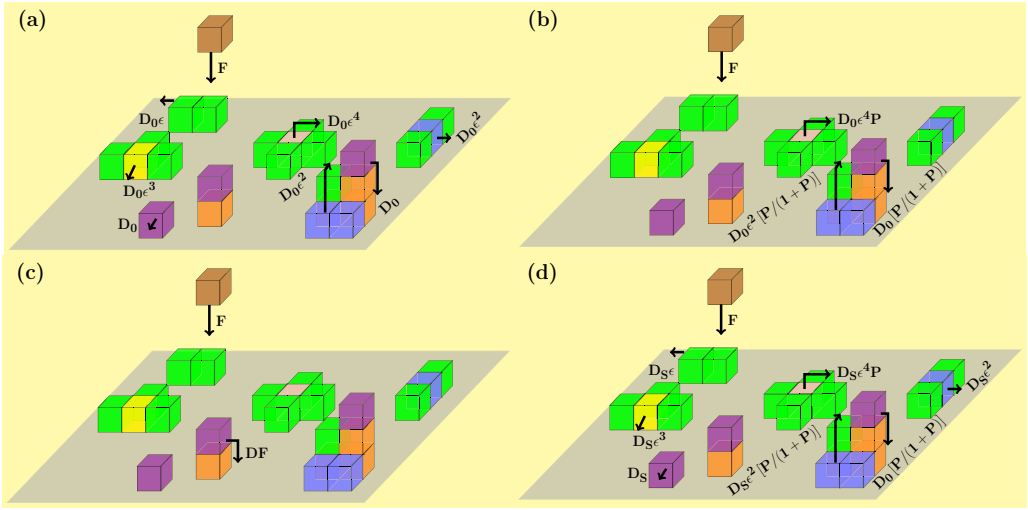

FIG. 1. Deposition models with collimated flux (brown particles) and some possible adatom hops. (a) (model 1) Standard CV model with adatom hopping rates depending on the numbers n of lateral neighbors [$n = 0$ (magenta), 1 (green), 2 (blue), 3 (yellow), and 4 (pink)] and with immobile subsurface adatoms (orange). (b) (model 2) CV model with ES barriers as defined in Eq. (4). (c) (model 3) DF of an adatom after adsorption. The collective diffusion follows the same rules of model 2. (d) (model 4) CV model with enhanced surface diffusion on the substrate ($D_S > D_0$).

Model 2. CV model with ES barrier for interlayer hops.

The ES barrier is an increase in the activation energy for adatoms to cross step edges, i.e., to execute interlayer hops. It is observed in the deposition of metals, semiconductors, organic molecules, and colloidal particles [46–49]. The inclusion of ES barriers in the CV model leads to the nucleation and uncorrelated growth of mounds whose average widths increase with the temperature (for growth at constant temperature). The surface roughness increases as $t^{1/2}$ at very long times, but there may be an initial layer-by-layer growth [41]. Applications to oxide and sulfide films [50,51] were recently suggested [41].

This model also considers the hopping rate of Eq. (1) for intralayer hops, i.e., hops where the position z does not change. However, for interlayer hops, the rate is multiplied by a probability $P_{\rm hop}$ that depends on the height difference Δh between the current column and the target column. Following the reasoning of Leal *et al.* [52] for implementing ES barriers in the SC lattice, we set

$$P_{\rm hop} = \frac{P}{1 + P(|\Delta h| - 1)}, \tag{4}$$

where

$$P = \exp\left[-E_{\rm ES}/(k_B T)\right], \tag{5}$$

and $E_{\rm ES} > 0$ is the energy barrier at the step edge separating the two columns.

Figure 1(b) show some adatom hops that highlight the difference from model 1 [Fig. 1(a)] in the same landscape. Observe that $P_{\rm hop} = P$ for a monolayer step, while $P_{\rm hop} < P$ for higher steps accounts for possible effects of a diffusion in a vertical wall which is hidden in the model [52]; this is important due to the growth of mounds with increasing slopes [41].

Model 3. CV model with ES barrier and downward funneling (DF).

DF is a transient relaxation mechanism, i.e., a relaxation restricted to a short time interval after the incidence of an atom. It is an effect of the increased vertical momenta of the incoming atoms as they approach the film surface [32]. While the ES barrier favors the formation of increasingly larger local slopes, the DF counterbalances this effect by reducing the slope at the point of incidence of each atom. The consequence is the growth and coarsening of mounds with approximately constant, temperature-dependent slopes [42]. This morphology is observed in films of several metals [4–6].

To simulate the DF mechanism when the atom reaches the top of a (randomly chosen) column (x, y), a neighboring column [$(x \pm 1, y)$ or $(x, y \pm 1)$] is randomly chosen and the atom moves to that column if its height is smaller than that of the incidence one, otherwise it remains at column (x, y). Figure 1(c) illustrates the DF of an incident atom. After relaxation by DF, the thermally activated diffusion of the adatom occurs as in model 2; see Fig. 1(b).

In the mounded surfaces produced with this model, the height difference Δh between neighboring columns is generally small [42]. Thus, similar results are obtained if the interlayer hopping rate is multiplied by $P_{\rm hop}$ in Eq. (4), as adopted here, or if $P_{\rm hop} = P$ is considered for all height differences [42].

In models 1, 2, and 3, the hopping rates do not depend on z but only on height differences. This is suitable to represent deposition on a substrate of the same crystalline material (homoepitaxial growth). After the substrate is covered by several layers, the model may also represent heteroepitaxial growth features if strain effects can be neglected.

Model 4. Extended CV model for growth on a foreign substrate.

Here, we consider the CV model in which adatom diffusion coefficients on the substrate are larger than the coefficients in upper layers of the deposit, but ES barriers are neglected and no transient relaxation (such as DF) is considered [14]. These

features favor the formation of islands which simultaneously grow in all directions [18]; after these islands coalesce, a continuous film with relatively smoother surface is formed. The initial roughness evolution qualitatively agrees with those of perovskite films deposited on Si [12,13], CdTe films deposited on a polymeric substrate [14], and mixed organic films deposited on amorphous SiO_x[15]. The same is expected in heteroepitaxy with formation of multilayer islands if strain effects are sufficiently weak (consistently with the model hypothesis of uniform interactions in all layers of the deposit except the first one) [18].

The model considers the same hopping rates of model 1, Eq. (1), for adatoms at points with $z > 1$ (adatoms on the film). However, adatoms at $z = 1$ (on the substrate) with N lateral NNs have hopping rate

$$D' = D_S \epsilon^N, \tag{6}$$

with

$$D_S = \nu \exp\left[-E_S/(k_B T)\right], \quad 0 < E_S < E_A. \tag{7}$$

The above relation between the activation energies E_S and E_A physically represents a weaker atom-substrate interaction in comparison with the interaction between atoms of the deposited material [14,18]. It implies $D_S > D_0$, which leads to a net adatom flux to high layers of the islands; otherwise, if $E_S \geqslant E_A$, there is no such flux and layer by layer growth is expected (similar to model 1) [18]. Figure 1(d) shows adatom hops that highlight the difference from model 1 [Fig. 1(a)] in the same landscape.

The deposition conditions in all models are characterized by two common dimensionless parameters, which are the diffusion-to-deposition ratio on terraces

$$R = \frac{D_0}{F} = \tilde{\nu} \exp\left[-E_A/(k_B T)\right], \quad \tilde{\nu} = \frac{\nu}{F}, \tag{8}$$

and the factor ϵ [Eq. (3)] which is interpreted as a detachment probability per lateral NN. In models 2 and 3, a third dimensionless parameter is the ES probability P [Eq. (5)]. In model 4, no ES barrier is considered ($P_{\text{hop}} = 1$), the parameter R is defined only at $z > 1$, and an additional parameter is the diffusion-to-deposition ratio on the substrate:

$$R_S = \frac{D_S}{F} = \tilde{\nu} \exp\left[-E_S/(k_B T)\right], \tag{9}$$

where $R_S > R$.

A summary of the rules of the four deposition models and of the main morphological features of the films grown at constant temperature are presented in Table I.

TABLE I. Summary of model rules and consequent surface features.

Model	Summary	Surface features in growth at constant temperature (asymptotic)
1	Growth without ES barrier, same substrate	Kinetic roughening (VLDS class)
2	Growth with ES barrier, same substrate	Uncorrelated mound growth
3	ES barrier and downward funneling, same substrate	Mound coarsening with slope selection
4	Growth on foreign substrate without ES barrier	Multilayer island growth; coalescence with maximal roughness; smoother continuous film

B. Quantities of interest

The number of deposited monolayers (MLs) or dimensionless film thickness at time t is

$$\theta = Ft. \tag{10}$$

The thickness fluctuations are characterized by the surface roughness

$$W = \sqrt{W_2} = \langle (\,\overline{\tilde{h}^2}\,) \rangle^{1/2}, \quad \tilde{h} \equiv h - \overline{h}, \tag{11}$$

where the overbars denote a spatial average over the (x, y) columns and the angular brackets denote an average over different configurations with a given thickness.

In films grown with models 1, 2, and 3 at constant temperature, the roughness monotonically increases with the thickness; however, if R and ϵ are sufficiently large (typical of high temperature growth) and the ES barrier is small, initial layer-by-layer growth is observed, and the roughness oscillates with values $W < 1$. Asymptotically, the roughness increases as a power law of the thickness, $W \sim \theta^\beta$, where β is called the growth exponent. This exponent is independent of the model parameters, and the known values are $\beta \approx 0.2$ (VLDS class) for model 1 [45,53,54], $\beta = 1/2$ (statistical growth) for model 2 [8,41], and $\beta = 1/4$ (mound coarsening with slope selection) for model 3 [7,42]. However, in the thickness ranges analyzed in this work, most asymptotic behaviors were not attained yet, so a comparison of exponent values is not adequate to interpret our results.

Model 4 with $R_S \gg R$ shows a nonmonotonic roughness evolution. At short times, islands with two or more layers are formed [18] and the roughness increases, but it reaches a maximal value and decreases as the islands coalesce, and a continuous film (with much smaller roughness) is formed [14,54].

C. Simulation details

The model parameters considered here are similar to those considered in recent simulational studies [41,42,45,53,54] for two reasons: (i) they provide the typical morphologies summarized in Table I; and (ii) their ranges are representative of metal and semiconductor films, such as those reported in Ref. [10].

In all simulations, we consider the typical frequency $\nu = 10^{13}\text{s}^{-1}$ for the thermally activated processes and a small flux $F = 0.1\text{s}^{-1}$, which leads to $\tilde{\nu} = 10^{14}$ in Eq. (8). The maximal deposited thickness ranged from $\theta_{\max} = 10^2$ to $\theta_{\max} = 10^3$; for films of atoms or small molecules, they roughly correspond to thicknesses from 20 nm to 2 μm.

Table II shows the simulated parameter sets. For model 1, the sets are labeled from 1.1 to 1.3 according to the activation energies E_A and E_B. For model 2, the sets are labeled from 2.1

TABLE II. Sets of activation and binding energies and temperatures used in the simulations. E_S and R_S are relevant only in model 4, otherwise they have the respective values of E_A and R.

Set	E_S(eV)	E_A(eV)	E_B(eV)	E_{ES}(eV)	T (K)	R_S	R	ϵ	P
1.1		0.6	0.5	0.0	[230, 300]		$[7.1, 8.3 \times 10^3]$	$[1.11 \times 10^{-11}, 3.99 \times 10^{-9}]$	1
1.2		0.6	0.09	0.0	[230, 300]		$[7.1, 8.3 \times 10^3]$	$[1.06 \times 10^{-2}, 3.08 \times 10^{-2}]$	1
1.3		0.6	0.058	0.0	[230, 300]		$[7.1, 8.3 \times 10^3]$	$[5.36 \times 10^{-2}, 0.11]$	1
2.1		1.0	0.3	0.10	[500, 600]		$[8.3 \times 10^3, 4.0 \times 10^5]$	$[9.5 \times 10^{-4}, 3.0 \times 10^{-3}]$	[0.098,0.14]
2.2		1.0	0.3	0.15	[500, 600]		$[8.3 \times 10^3, 4.0 \times 10^5]$	$[9.5 \times 10^{-4}, 3.0 \times 10^{-3}]$	[0.030,0.055]
2.3		1.0	0.3	0.25	[500, 600]		$[8.3 \times 10^3, 4.0 \times 10^5]$	$[9.5 \times 10^{-4}, 3.0 \times 10^{-3}]$	[0.0030,0.0079]
3.1		1.0	0.3	0.10	[500, 600]		$[8.3 \times 10^3, 4.0 \times 10^5]$	$[9.5 \times 10^{-4}, 3.0 \times 10^{-3}]$	[0.098,0.14]
3.2		1.0	0.3	0.15	[500, 600]		$[8.3 \times 10^3, 4.0 \times 10^5]$	$[9.5 \times 10^{-4}, 3.0 \times 10^{-3}]$	[0.030,0.055]
3.3		1.0	0.3	0.25	[500, 600]		$[8.3 \times 10^3, 4.0 \times 10^5]$	$[9.5 \times 10^{-4}, 3.0 \times 10^{-3}]$	[0.0030,0.0079]
4.1	0.7	1.0	0.3	0.0	[500, 600]	$[8.8 \times 10^6, 1.3 \times 10^8]$	$[8.3 \times 10^3, 4.0 \times 10^5]$	$[9.5 \times 10^{-4}, 3.0 \times 10^{-3}]$	1.0
4.2	0.6	0.9	0.3	0.0	[500, 600]	$[8.9 \times 10^7, 9.1 \times 10^8]$	$[8.5 \times 10^4, 2.7 \times 10^6]$	$[9.5 \times 10^{-4}, 3.0 \times 10^{-3}]$	1.0

to 2.3 according to the activation energies E_A, E_B, and E_{ES}. For model 3, the parameters of the simulated sets (3.1, 3.2, and 3.3) are the same of model 2; the difference is the introduction of DF. For model 4, the sets are labeled 4.1 and 4.2 according to E_A, E_S, and E_B. In models 1, 2, and 3, there is no difference in diffusion on the substrate and on the film, so $R_S = R$. In models 1 and 4, there is no ES barrier ($E_{ES} = 0$, $P = 1$).

If the temperature is varied during the deposition, an initial temperature T_I is set at $\theta = 0$, and a final temperature T_F is set at the maximal deposited thickness θ_{max}. The values of θ_{max} vary from 10^2 ML (one of the cases of model 4) to 10^4 ML (model 1). We assume that the temperature linearly changes in time during the deposition; since the atomic or molecular flux is constant, this implies a linear variation with the thickness θ. For the implementation in the simulations, the temperature is changed when the thickness reaches an integer value ($\theta = 1, 2, \ldots, \theta_{max} - 1$), but it is maintained constant during the subsequent deposition of one monolayer (L^2 adatoms). The corresponding thickness-dependent temperature is

$$T(\theta) = T_I + \frac{\lfloor \theta \rfloor}{\theta_{max}}(T_F - T_I), \tag{12}$$

where $\lfloor \theta \rfloor$ denotes the floor function of (greatest integer less than or equal to) θ.

Figure 2 schematically illustrates a case of time-increasing temperature. Observe that the highest temperature at which the growth actually occurs (the deposition of the last monolayer) is slightly below T_F. For the variations considered here, in which $\Delta T/\Delta\theta < 1$ K/ML, these details become irrelevant because the film properties are quite similar at temperatures differing by 1 K or less.

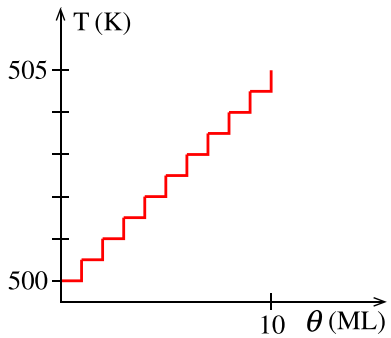

FIG. 2. Growth temperature as a function of the thickness with $T_I = 500$ K, $T_F = 505$ K, and $\theta_{max} = 10$ ML.

The lateral size of the simulated deposits is $L = 1024$ (in lattice units), which is large enough to avoid finite-size effects on the simulation data, as shown in recent work [41]. For each parameter set, configurational averages are obtained from 10 to 100 deposits. The KMC algorithm described in recent work [41] was implemented on available computers with Threadripper 2970WX and Ryzen 5950X processors.

III. RESULTS

A. Interpolation of the roughness evolution

In a simplified version of the CV model (model 1) with $\epsilon = 0$, simulations at several temperatures provided an approximate roughness function $W_A(T, \theta)$ [55], which is applicable for films with thickness θ under the assumption that they grew at a constant temperature T at all times. In a subsequent study of this model with time-varying temperature, the roughness data could be reasonably fit by $W_A(T, \theta)$ [21]. This means that, for each temperature, the film reaches a configuration which is characteristic of that temperature and of the current thickness, independently of the growth history.

In this work, we check whether the same is possible in the models 1 to 4. However, we could not obtain reliable roughness functions for these models in broad ranges of parameters, so we adopt a different method. For each model, KMC simulations were performed in some temperature sets and in a chosen thickness range. From these data, an interpolated roughness function $W_I(T, \theta)$ is built for the films that grew with all intermediate temperatures T (i.e., temperatures between the minimal and the maximal temperatures in the simulated range) and all thickness θ in the chosen range.

The interpolation method is illustrated here with the parameter set 1.1 of model 1; see model features in Table I and set details in Table II. Figure 3(a) shows the evolution of the roughness during the deposition of films maintained at constant temperatures from 230 K to 300 K in intervals of 10 K; decreasing roughness is obtained as the temperature increases, as shown in previous works [45]. To estimate the surface

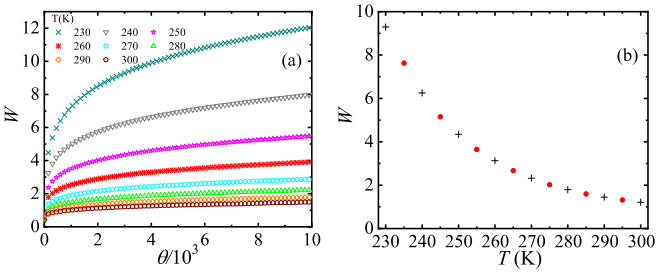

FIG. 3. (a) W as a function of θ obtained in simulations at constant temperatures (indicated in the plot) with parameter set 1.1. (b) W as a function of T at thickness $\theta = 3000$ ML obtained in simulations (black crosses) and $W_I(T, \theta)$ for some intermediate temperatures obtained by the second-order Lagrangian interpolation method (red dots).

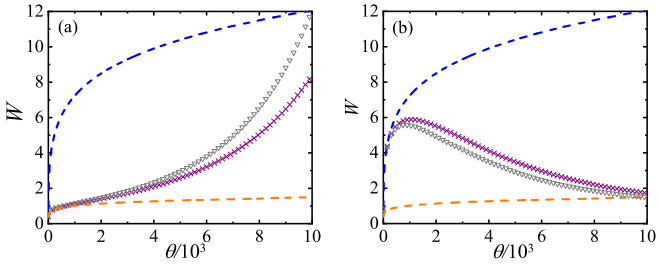

FIG. 4. W versus θ obtained in KMC simulations with (a) time-decreasing and (b) time-increasing temperature, with parameter set 1.1 (purple crosses). Both plots also show W_I obtained with the interpolation method (gray triangles) and W obtained in deposition at constant temperatures 230 K (blue dashed line) and 300 K (orange dashed line).

roughness at a given thickness θ and at temperatures not directly sampled in the simulations, a quadratic interpolation procedure based on Lagrange polynomials is employed. First, for each temperature T, three neighboring temperatures (T_1, T_2, T_3) where simulations were performed are selected; for instance, if $T = 242$ K, then $T_1 = 230$ K, $T_2 = 240$ K, and $T_3 = 250$ K are selected. Using the roughness values measured at these three temperatures $[W(T_1, \theta), W(T_2, \theta), W(T_3, \theta)]$, the roughness at temperature T is then estimated as

$$W_I(T, \theta) = \sum_{i=1}^{3} W(T_i, \theta) \prod_{\substack{j=1 \\ j \neq i}}^{3} \left(\frac{T - T_j}{T_i - T_j} \right). \tag{13}$$

Now consider the roughness of a film with thickness $\theta = 3000$ ML at intermediate temperatures in the range $235\text{K} \leqslant T \leqslant 295$ K and in intervals of 10 K, which are not directly sampled in the simulations of Fig. 3(a). The simulated data and some of the interpolated results are presented in Fig. 3(b). This procedure enables consistent interpolation over a continuous temperature range and is similarly applied to other values of T and θ within the bounds of the available data.

This interpolation method will be used to predict the roughness evolution of all models in time-varying temperature in the next subsections: for each integer value of the thickness θ, the temperature $T(\theta)$ is given by Eq. (12), and the interpolated roughness is $W_I(T(\theta), \theta)$. The results will be compared with direct KMC simulations in time-varying temperature.

B. Growth with model 1 and time-varying temperature

Figures 4(a) and 4(b) show W versus θ obtained in KMC simulations with parameter set 1.1 with time-increasing and time-decreasing temperature, respectively. The films have maximal thickness 10^4 ML and the limiting temperatures are 230 K and 300 K; see Table II. Figures 4(a) and 4(b) also show the prediction of the interpolation of constant temperature deposition data, $W_I(T, \theta)$, and the roughness evolutions when the limiting temperatures are kept constant (observe that the initial and final values of the interpolated curves agree with these limiting temperature data).

For time-increasing temperature, the interpolation results closely match the values obtained in KMC simulations. Both show a nonmonotonic roughness variation in which initial roughening (at the lowest temperatures) is followed by smoothening (at the highest temperatures). For time-decreasing temperature, both methods lead to monotonic roughness increase, but the simulations give significantly smaller roughness. Thus, the interpolation method only has qualitative agreement with the simulations, despite the very slow variation of the temperature (less than 0.01 K per ML).

Figures S1 and S2 of the Supplemental Material [56] show similar trends for growth with parameter sets 1.2 and 1.3; see set details in Table II. These results confirm that, for model 1, the interpolation of constant temperature results can be used to predict the qualitative trend of the roughness evolution in time-varying temperature, but there may be quantitative deviations. These deviations imply that the surface fluctuations strongly depend on the growth history, even if the temperature variation is very slow. This result contrasts with those formerly obtained in a simpler film growth model with irreversible aggregation to lateral neighbors (model 1 with $\epsilon = 0$), in which similar rates of temperature variation (less than 0.01 K per ML) were considered [21].

C. Films with uncorrelated mound growth (model 2)

Figure 5(a) shows W versus θ for films grown with parameter set 2.1 (see Table II) at constant temperatures between 500 K and 600 K and maximal thickness of 500 ML (which is still far from the asymptotic scaling). For a given thickness, the roughness decreases as the temperature increases.

Figures 5(b) and 5(c) show top views and vertical cross sections of films grown at the lowest temperature, 500 K, and thicknesses 100 ML and 500 ML, respectively; Figs. 5(d) and 5(e) show cross sections of films grown at the highest temperature, 600 K, and the same thicknesses. At 500 K, the 100 ML film has mounds of widths ∼20 ML, which grow with deep gaps between them. The film surface with 500 ML remains with high asperity at short length scales. Instead, at 600 K, the 100 ML film has a smooth surface with wide bumps, which, in the 500 ML film, give rise to smooth, rounded mounds (widths ∼80 ML). The top views of Figs. 5(b)–5(e) show no coarsening of these mounds, i.e., uncorrelated mound growth.

The roughness evolutions of films grown with the same parameter set 2.1 but with time-decreasing temperature (from 600 K to 500 K) and time-increasing temperature (from 500 K

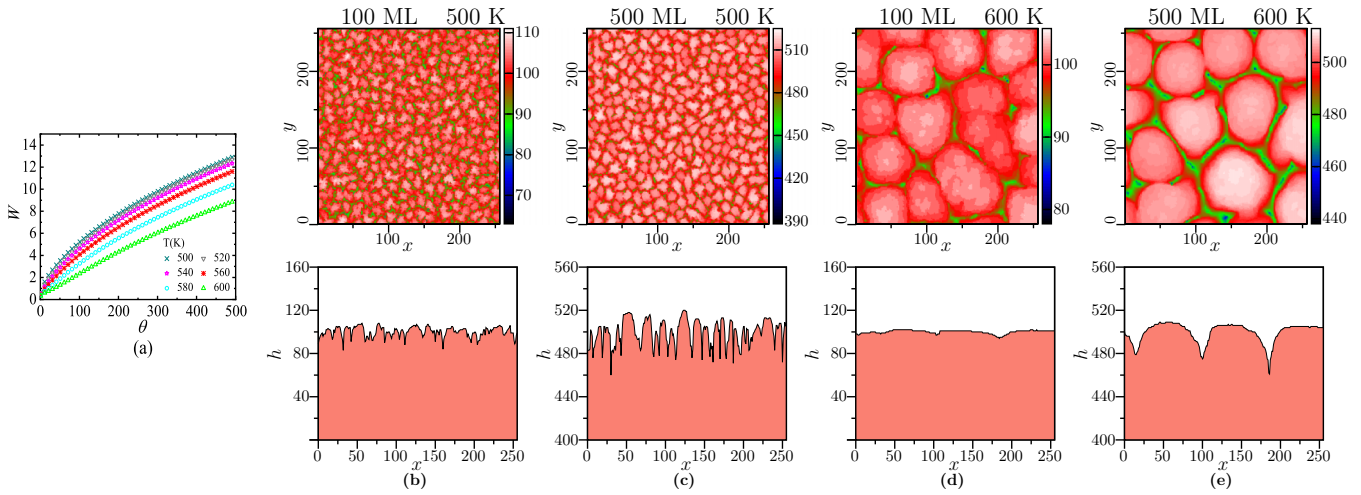

FIG. 5. (a) W versus θ obtained in KMC simulations at constant temperatures (indicated in the plot) with parameter set 2.1. (b)–(e) Top views and vertical cross sections of films grown in those simulations at the indicated temperatures and thicknesses.

to 600 K) are shown in Figs. 6(a) and 6(b), respectively. The curves for growth at the limiting temperatures and the estimates of the interpolation method are also shown. For time-decreasing temperature, the interpolation data closely matches the direct simulation data until 200 ML, and they deviate up to ∼10% in larger thicknesses. For time-increasing temperature, the simulations and the interpolation method predict nonmonotonic evolution of the roughness, but their data significantly differ after 100 ML. Again, the interpolation method is an interesting predictor of a nontrivial roughness evolution, but the quantitative deviations may be large.

The striking feature in the case of time-increasing temperature is that the final roughness obtained in direct simulations, ≈5 ML, is much smaller than the value predicted by the interpolation, ≈9 ML, which is the value that would be obtained if the highest temperature were kept constant at all times. Moreover, comparison with Fig. 5(a) shows that the 500 ML films deposited with time-increasing temperature are smoother than all films with the same thickness deposited at constant temperature in the same range.

Figures 7(a)–7(e) show top views and vertical cross sections during film growth with decreasing temperature (from $T_I = 600$ K to $T_F = 500$ K) and with parameter set 2.1. The surface develops some bumps at 50 ML and, at 100 ML, the bumps are more pronounced than those observed in growth at constant $T = 600$ K and the same thickness [Fig. 5(d)]. Subsequently, those bumps form mounds with increasing internal asperity. At 500 ML, the surface configuration has a long wavelength envelope characteristic of growth at the highest temperatures [a little narrower than the mounds of Fig. 5(e)] and short wavelength fluctuations characteristic of growth at the lowest temperature [compare with Fig. 5(c)]. This final configuration is rougher than those of films with the same thickness obtained at any of those temperatures.

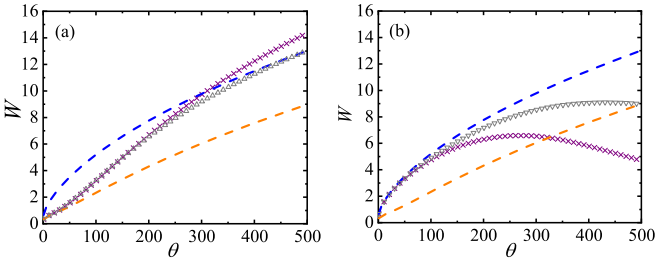

FIG. 6. W versus θ obtained in KMC simulations with (a) time-decreasing and (b) time-increasing temperature, with parameter set 2.1 (purple crosses). Both plots also show W_I obtained with the interpolation method (gray triangles) and W obtained in simulations of growth at constant temperatures 500 K (blue dashed line) and 600 K (orange dashed line).

Figures 8(a)–8(e) show top views and vertical cross sections of films with several thicknesses that grew with increasing temperature, from $T_I = 500$ K to $T_F = 600$ K, and with parameter set 2.1. The initial surface has narrow mounds which are similar to those of growth at constant $T = 500$ K; e.g., compare 100 ML profiles in Figs. 5(b) and 8(b). Subsequently, the film evolves with coarsening of those mounds due to the temperature increase, in contrast with the uncorrelated mound growth observed when the temperature was kept constant [Figs. 5(b) and 5(c)]. The final configuration [Fig. 8(e)] shows large plateaus with gaps that contribute to the roughness of ≈5 ML. These gaps are less deep than those of 500 ML films grown at constant $T = 600$ K [Fig. 5(e)], where the roughness ≈9 ML was almost the double.

Figures S3–S10 of the Supplemental Material [56] show similar roughness evolutions and surface patterns for films grown with parameter sets 2.2 and 2.3; see set details in Table II. The final roughness of films deposited at time-increasing temperature (purple crosses in the $W \times \theta$ plots) also has smoother final configurations than those produced when the highest temperature was kept constant (dashed orange lines in the same plots). This smoothening occurs because the increasing temperature leads to increasing diffusion lengths of the adsorbed atoms, which can consequently fill the gaps between the narrow mounds developed at the beginning of the growth. In other words, the temperature increase leads to coarsening of the initially formed mounds. A quantitative analysis based on the expected adatom diffusion lengths is postponed to Sec. IV.

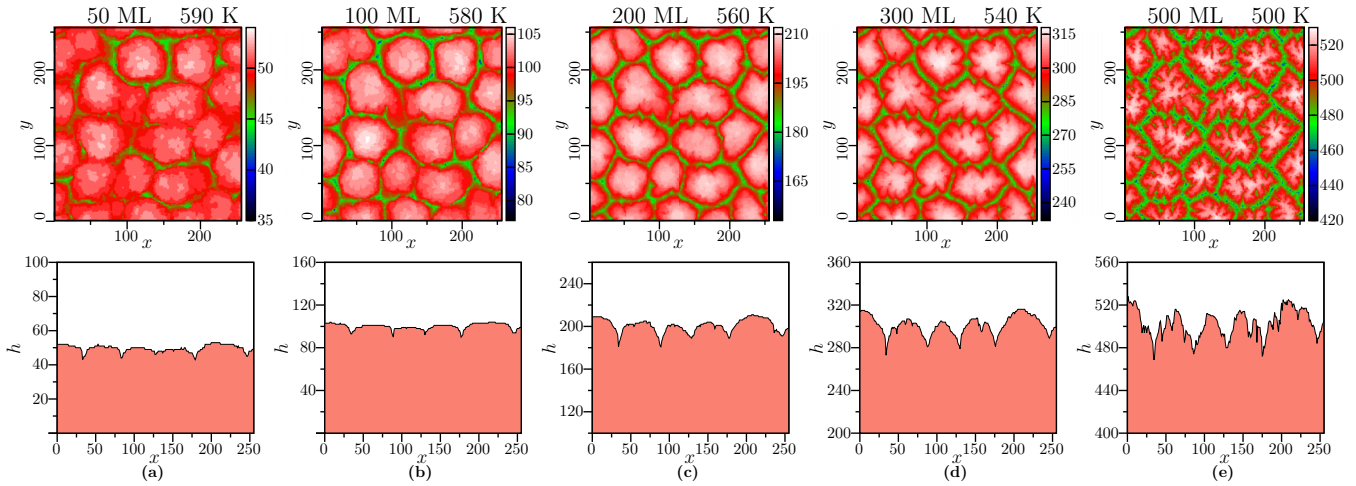

FIG. 7. Top views and vertical cross sections of films grown in simulations with parameter set 2.1 and a linear temperature decrease from $T_I = 600$ K to $T_F = 500$ K [roughness evolution in Fig. 6(a) (purple crosses)]. The thicknesses and the corresponding temperatures are indicated in all plots.

D. Films with mound coarsening (model 3)

At constant growth temperature, the combination of ES barriers and DF of incident atoms leads to nucleation and coarsening of mounds whose slopes depend only on the intralayer diffusion parameters (R and ϵ) [42]; see model summary in Table I. However, at short deposition times, the effects of DF and ES barriers are weak because the film roughness is small. Thus, in films grown at constant temperature, the choice of a higher temperature leads to the formation of smoother surfaces. This is confirmed in the $W \times \theta$ plot of Fig. 9(a) and thicknesses $\lesssim 50$ ML, which is obtained in simulations with parameter set 3.1; see Table II. As the films thicken, the DF suppresses large height differences between neighboring columns and controls the instability that the ES barrier could develop (in contrast with model 2). In the largest thickness of 500ML, a larger roughness is observed for a higher growth temperature. Figures 9(b) and 9(c) show cross sections of the 500 ML deposits grown at constant temperatures, 500 K and 600 K, respectively, and confirm that wider and taller mounds are formed at the highest temperature.

The roughness evolutions of films grown with model 3.1 with time-decreasing and time-increasing temperature are shown in Figs. 10(a) and 10(b), respectively. The curves predicted by the interpolation approach and those obtained in simulations with the limiting temperatures (500 K and 600 K) kept constant are also shown. The interpolation curves agree with the results of time-varying simulations until ∼100MLs, in which the roughness is small ($W \lesssim 1$), but there are qualitative differences for larger thicknesses: in Fig. 10(a), the interpolation predicts a roughness peak which is not observed in the simulations; in Fig. 10(b), it fails to predict the roughness peak shown in the simulations.

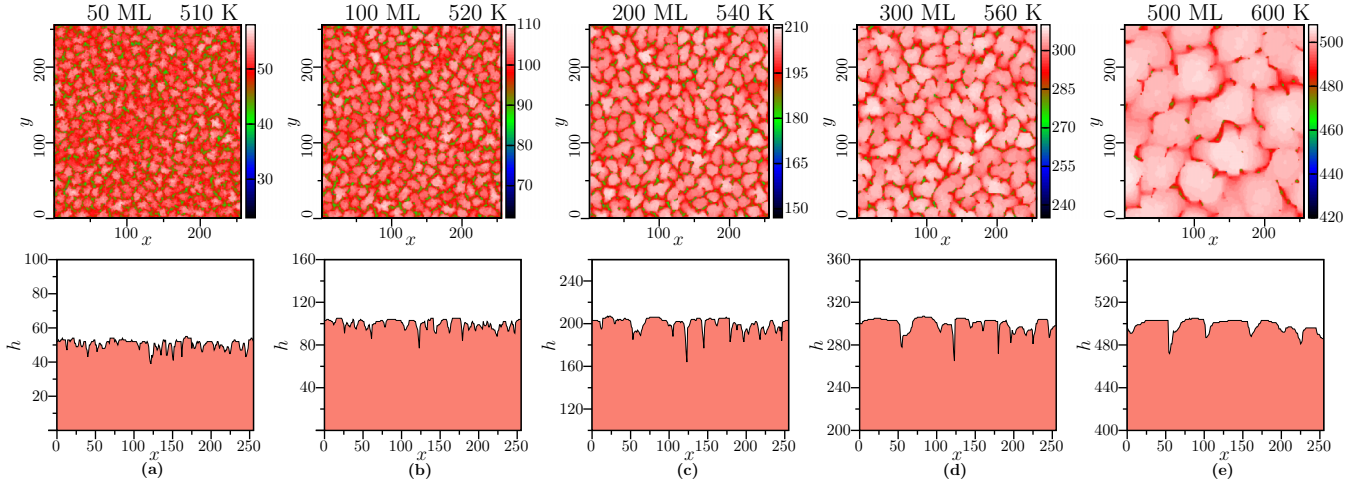

FIG. 8. Top views and vertical cross sections of films grown in simulations with parameter set 2.1 and a linear temperature increase from $T_I = 500$ K to $T_F = 600$ K [roughness evolution in Fig. 6(b) (purple crosses)]. The thicknesses and the corresponding temperatures are indicated in all plots.

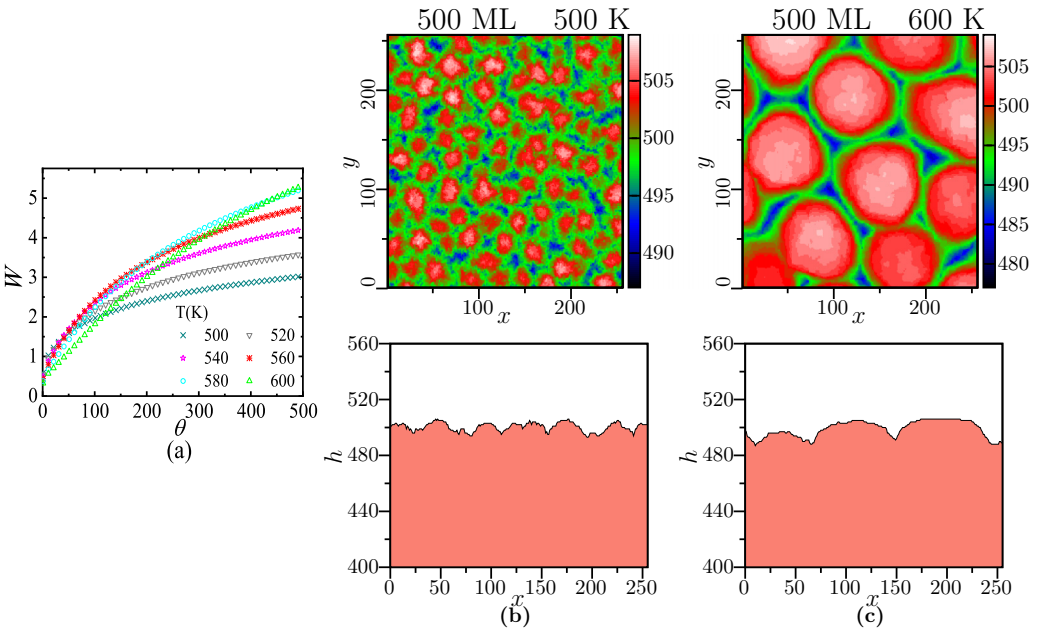

FIG. 9. (a) W versus θ obtained in KMC simulations at constant temperatures (indicated in the plots) with parameter set 3.1. (b), (c): Top views and vertical cross sections of 500 ML films grown with set 3.1 at 500 K and 600 K, respectively.

The films deposited at time-decreasing temperatures are much rougher than those obtained in constant temperature deposition; Fig. 10(a). Vertical cross sections of the films grown in time-decreasing temperature are shown in Fig. S11 of the Supplemental Material [56]. With ∼100–200 ML, they have wide mounds characteristic of the largest temperatures, but the internal asperity of those mounds increases as the film thickens in lower temperature conditions. The situation is similar to that of uncorrelated mound growth in time-decreasing temperature, as illustrated in Figs. 7(a)–7(e) for the set 2.1.

The 500 ML films deposited in time-increasing temperature are only slightly smoother than those deposited at 500 K; Fig. 10(b). Vertical cross sections of the films grown in time-increasing temperature are shown in Fig. S12 of the Supplemental Material [56]. It reveals the formation of narrow mounds at the beginning of the growth (∼100 ML) and their rapid coarsening as the growth continues and the temperature increases. However, due to the mound slope selection characteristic of model 3, the heights and widths of the mounds tend to increase at the same rate. The competition of these mechanisms that respectively favor smoothening and roughening explains the small variation of the roughness between 200 ML and 500 ML shown in Fig. 10(b).

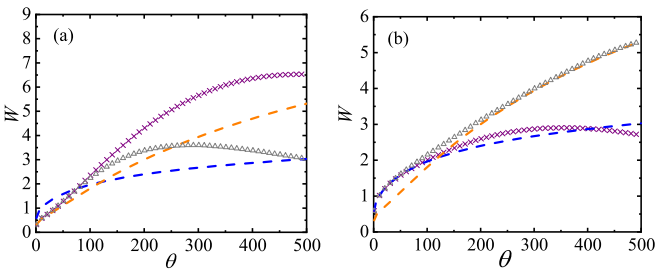

FIG. 10. W versus θ obtained in KMC simulations with (a) time-decreasing and (b) time-increasing temperature, with model 3.1 (purple crosses). The plot also shows W obtained with the interpolation method (gray triangles) and in simulations at constant temperatures 500 K (blue dashed line) and 600 K (orange dashed line).

Figures S13–S20 of the Supplemental Material [56] show roughness evolutions and selected profiles of films grown with parameter sets 3.2 and 3.3; see set details in Table II. The growth at time-varying temperature (purple crosses in the $W \times \theta$ plots) leads to final configurations with intermediate roughness between the values obtained in growth at the two limiting temperatures (dashed curves in those plots). The $W \times \theta$ curves obtained by interpolation of constant temperature results also disagree with the simulation data.

Thus, if the growth exhibits mound coarsening with slope selection, in which the increase of the temperature produces wider and taller mounds (and consequently larger roughness), two conclusions can be drawn. First, the surface diffusion is unable to reorganize the film surface in a way that the fluctuations weakly depend on that variation, which explains the qualitative discrepancies between the simulation and the interpolation results. Second, the time-increasing temperature does not lead to a significant decrease in the roughness when compared with constant temperature deposition. Thus, the temperature control during the deposition is not a suitable tool for smoothening the film surface in cases of mound coarsening with slope selection.

E. Growth and coarsening of islands on foreign substrates (model 4)

In growth with model 4, roughness usually has a peak as a function of the thickness, in contrast with the continuous

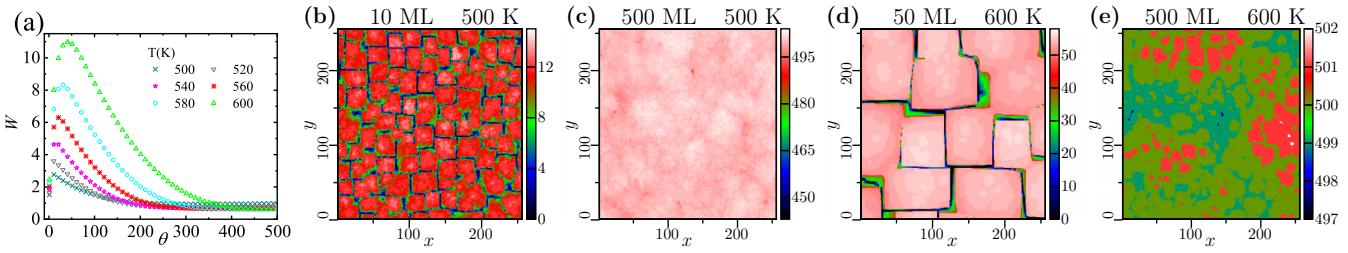

FIG. 11. (a) W versus θ from KMC simulations at constant temperatures (indicated in the plots) with parameter set 4.1. (b)–(e): Top views of the film surfaces obtained in those simulations at the indicated temperatures and thicknesses. The color maps show heights relative to the minimum in each image.

roughening of the previous models; see model summaries in Table I. This is confirmed in Fig. 11(a), which shows W versus θ for films grown with model 4.1 (see Table II) and several temperatures which are kept constant during the deposition. At short times, the increased adatom diffusion coefficient on the substrate ($z = 1$) leads to a high flux to the upper layers of the initial islands [18], which grow with large average heights; this explains the roughness increase. However, when those islands coalesce, an extended film with a smooth surface is formed, which explains the roughness decrease [14,54]. If the growth temperature increases, the flux to the upper layers increases, taller islands are formed, and the roughness peak is higher [54].

Figures 11(b)–11(e) show top views of deposits grown at the limiting temperatures (500 K and 600 K) and two thicknesses, one near the maximal roughness (10 ML for 500 K, 50 ML for 600 K) and the other of 500 ML (cross sections are not shown in this case because they are very different for different vertical planes). These images illustrate the correlation between the roughness peak and the island coalescence. The height scales show that wider islands (grown at the larger temperature) are also taller, which explains the higher roughness peaks.

Figures 12(a) and 12(b) show W as a function of θ obtained in simulations of model 4.1 with time-decreasing and time-increasing temperature, respectively. The curves predicted by the interpolation approach and those obtained in simulations at the limiting temperatures are also shown. The interpolation curves agree with the results of time-varying simulations before the maximal roughness, but fail for larger

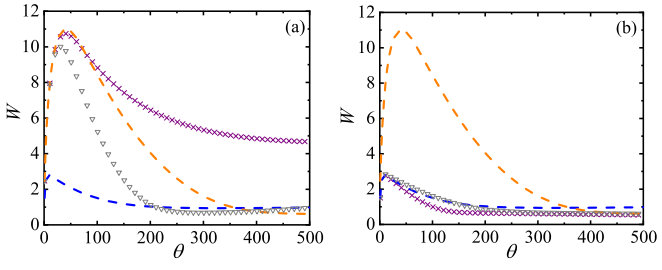

FIG. 12. W versus θ obtained in KMC simulations with (a) time-decreasing and (b) time-increasing temperature, with parameter set 4.1 (purple crosses). The plots also show W_I obtained with the interpolation method (gray triangles) and W obtained in simulations of growth at constant temperatures 500 K (blue dashed line) and 600 K (orange dashed line).

thicknesses, showing again that the features of constant temperature growth cannot be used to predict how the film evolves with time-varying temperature.

The films grown with time-decreasing temperature have larger roughness than those produced in constant temperature deposition [Fig. 12(a)]. Figures 13(a)–13(e) show top views of these films with several thicknesses. The deposit with 50 ML [Fig. 13(b)] has a pattern of coalesced islands separated by narrow gaps similar to that produced at the highest temperature, 600 K, and the same thickness [Fig. 11(d)]. However, the temperature decrease slows down the filling of those gaps, so they are still present in the 500 ML films [Fig. 13(e)]; this contrasts with the smooth surface of the film grown at constant temperature, 600 K, and the same thickness [Fig. 11(e)].

Instead, Fig. 12(b) shows that films grown with time-increasing temperature have smaller roughness than those grown at the limiting temperatures. Figures 14(a)–14(e) show top views of these films with several thicknesses. The multilayer islands formed on the substrate are small and rapidly coalesce to form a continuous film, similar to the growth at the lowest temperature, 500 K. After that, the growth proceeds as in model 1 (no ES barrier is present); the temperature increase leads to faster smoothening of the film surface in comparison with the smoothening at the initial temperature.

Many technological applications require film thicknesses below 100 nm, so here we also analyze the effect of time-increasing temperatures in films with a maximum of 100 ML. Figure 15 shows W versus θ for such films grown with set 4.1 using $T_I = 540$ K and $T_F = 600$ K. Observe that improved smoothening is obtained after 40–50 ML, although the roughness peak is slightly higher than that obtained in growth at a constant temperature of 540 K.

Figures S21–S24 of the Supplemental Material [56] show roughness evolutions and selected surface patterns of films grown with parameter set 4.2; see set details in Table II. They also show the benefit of increasing the temperature during the deposition to reduce the final roughness of the films. This process takes advantage of two features: (i) the large island density formed at a lower temperature leads to faster coalescence and smaller roughness peak in comparison with the deposition at a higher temperature; and (ii) the temperature increase leads to larger adatom diffusion lengths, which accelerates the filling of the gaps between the islands and the smoothening of the resulting continuous film. A quantitative treatment is also shown in Sec. IV.

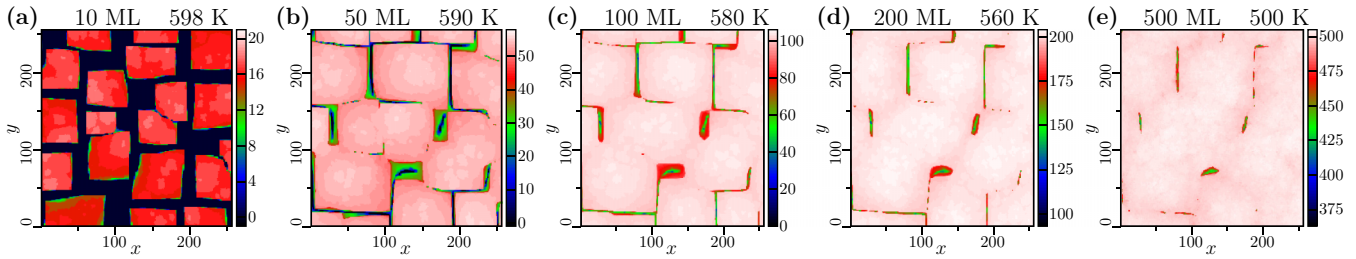

FIG. 13. Top views of film surfaces from simulations with parameter set 4.1, a linear temperature decrease from $T_I = 600$ K to $T_F = 500$ K, and thicknesses (a) 10 ML, (b) 50 ML, (c) 100 ML, (d) 200 ML, and (e) 500 ML. The color map represents the local height $h(x, y)$ of the interface.

IV. DISCUSSION

The deposition with models 2 and 4 and time-increasing temperature produced smoother films than the deposition at constant temperature, as shown in the plots of Figs. 6(b), S4(a), S8(a), 12, 15, and S22(a) (compare purple crosses for growth with increasing temperature and dashed lines for growth with constant temperature). This occurs due to an apparent coarsening of mounds or islands, which depends on the diffusion of adatoms deposited in those structures to the valleys separating them.

A recent study of the statistics of adatom diffusion during thin film deposition with model 1 showed that the average number of hops of an adatom is $\langle N\rangle \sim R^{0.38}$ in a low temperature regime characterized by almost irreversible attachment of those adatoms to lateral neighbors [57]. This regime is applicable whenever $R\epsilon^3 < 10^{-3}$, which encompasses all the simulations presented here. The corresponding diffusion length can be estimated as $l \sim \langle N\rangle^{1/2} \sim R^{0.19}$. Moreover, the distribution of the number of hops N is a stretched exponential in which the probability of a number of hops $5\langle N\rangle$ (i.e., 5 times larger than the average) is more than 10% of the probability of the average number $\langle N\rangle$. Thus, diffusion lengths that exceed l by a factor of 2 are frequently observed.

First, we apply these results to model 2.1, in which uncorrelated mounds grow (Sec. III C). The above characteristic sizes are estimated as $l \approx 5.6$ at 500 K, $l \approx 8.3$ at 550 K, and $l \approx 11.6$ at 600 K. The mound widths observed in the cross sections of Figs. 5(b)–5(e) at 500 K and 600 K are larger than these estimates of l, but the valleys between those mounds are much narrower than the mound widths. In the deposition with time-increasing temperature from 500 K to 600 K, the value of l at 550 K (250 ML) is ≈50% larger than that length at 500 K, which means that, at 550 K, adatoms are expected to move to distances ≈50% larger than the traveled distances at the beginning of the growth. This is sufficient for many atoms deposited on the narrow mounds to move to the valleys and fill them, which produces the coarsening illustrated in Figs. 8(a)–8(e). Interestingly, Fig. 6(b) shows that the thickness ≈250 ML, in which $T = 550$ K, is near the point where the roughness begins to decrease.

The case of multilayer island growth and coalescence of model 4.1 (Sec. III E) is more subtle. An important observation here is that the roughness peak appears when the islands have narrow gaps between them, and most of the incident atoms arrive at the island tops; for instance, Figs. 11(b) and 11(d) show gaps of widths 10 ML or less for growth at 500 K and 600 K, respectively. After the peak, the roughness decrease is associated with the motion of those atoms from the top of the islands to the gaps; importantly, after an adatom reaches the gap, its redistribution can be very fast due to the much larger diffusion coefficient on the substrate.

Following this reasoning, consider the deposition with time-increasing temperature from 540 K to 600 K; see Fig. 15. The roughness has a peak at thicknesses of 15–20 ML, and a mild smoothening is observed at ≈40 ML, both for deposition at 500 K or with increasing temperature. The diffusion lengths of the adatoms deposited on the island tops are: $l \approx 7.7$ ML at 500 K (beginning of the growth); $l \approx 9.2$ ML at 40 ML and $T = 564$ K (after the roughness peak); and $l \approx 11.7$ ML at 100 ML and $T = 600$ K (end of the growth). The ∼20% increase in l at a thickness of 40 ML explains why a more rapid filling of the gaps (which seldom have a width of 10 ML) begins at this point and accelerates during the deposition of the additional 60 ML. However, it is important to observe

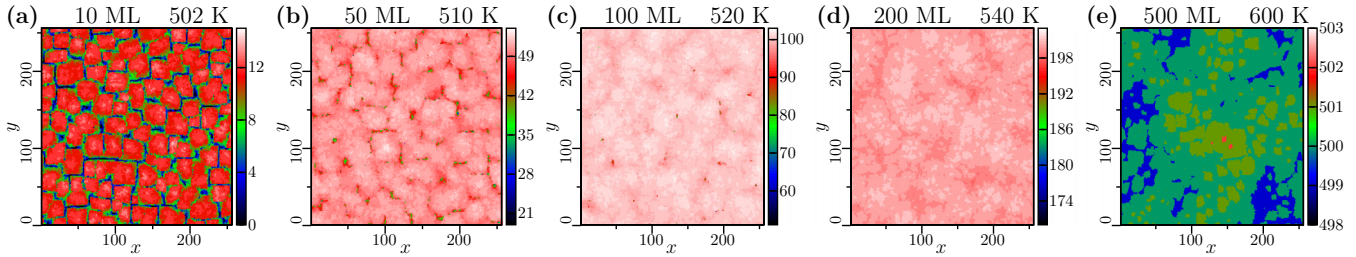

FIG. 14. Top views of film surfaces from simulation with parameter set 4.1, a linear temperature increase from $T_I = 500$ K to $T_F = 600$ K, and thicknesses (a) 10 ML, (b) 50 ML, (c) 100 ML, (d) 200 ML, and (e) 500 ML. The color map represents the local height $h(x, y)$ of the interface.

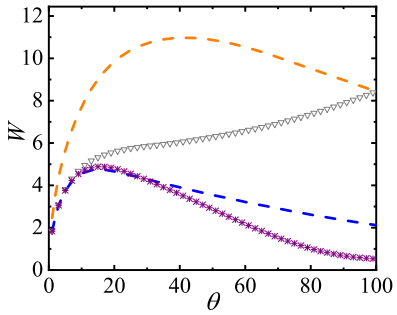

FIG. 15. W versus θ from KMC simulations with time-increasing temperature with parameter set 4.1 (purple crosses). The plot also shows W_E obtained with the interpolation method (gray triangles) and W obtained in simulations at constant temperatures 540 K (blue dashed line) and 600 K (orange dashed line).

that the rapid filling is possible because the islands are narrow, so a large fraction of incident particles is deposited near their borders and can move to the gaps. The same is difficult for the much wider islands grown at higher temperatures.

Thus, the film smoothening by temperature increase during the deposition is possible when a high density of mounds or islands appears at short times, which is the common feature of models 2 and 4. The temperature change leads to an increase in the diffusion lengths on the surface hills (upper layers) that allows filling of the valleys or gaps of those patterns. The sizes of the patterns grown at constant temperature can give hints on the temperature dependence of adatom diffusion lengths and can suggest how the temperature should vary for the smoothening to occur. In models of film growth, the results of previous studies may be used to obtain that temperature dependence [57].

The generalizability of this interpretation is warranted for several reasons. First, we studied four growth models that produce a variety of film surface morphologies at constant temperature, and these morphologies are experimentally observed in deposition from thermal vapor. Second, the absence of the smoothening effect in models 1 and 3 helped us to distinguish the morphological features which are associated with that effect (in models 2 and 4). Third, several sets of model parameters were considered in models 2 and 4, which shows that the smoothening effect is not a fortuitous event.

It is also important to observe that the temperature decrease during the deposition does not show the same advantages in the models studied here. This includes the films with mound coarsening and slope selection, in which larger roughness is obtained at higher temperatures (in growth at constant temperature).

In all models, we also showed that the interpolation of the surface roughness values obtained at constant growth temperature does not fit the results obtained in time-varying temperature. This contrasts with the good fits obtained in a previous work with a model in which adatom diffusion was allowed only on the film terraces, i.e., allowed only for adatoms without lateral neighbors [21]. The probable reason behind those successful fits is that the temperature change only affected the rate of motion of isolated adatoms, but did not lead to coarsening of mounds or islands. Instead, this coarsening is possible in all models studied here, which is a probable reason for the deviations from the interpolated roughnesses.

V. CONCLUSION

The deposition of thin films with time-varying temperature is studied with KMC simulations of four models that account for thermally activated diffusion of the adsorbed species as the relaxation mechanism. We were particularly interested in searching for conditions in which the temperature control could produce smoother film surfaces in comparison with the usual approach of deposition in constant substrate temperature. The chosen models show four different growth modes in constant temperature conditions: (1) kinetic roughening of the film surfaces; (2) growth of uncorrelated mounds whose widths increase with the temperature; (3) mound coarsening with selection of slopes that increase with the temperature; and (4) growth of multilayer islands on a foreign substrate and their coalescence to form a continuous film. These growth modes are observed in experiments with several materials.

The temperature variation during the deposition may lead to very different morphological evolutions of the films. This includes nonmonotonic variations of the roughness (an increase followed by a decrease) observed in models 1, 2, and 3 with both time-increasing and time-decreasing temperature, a feature which is not observed in constant temperature deposition with the same models.

However, our most important finding is that time-increasing temperature may reduce the film roughness by a significant factor in two of the studied models (2 and 4) in comparison with the deposition at any constant temperature in the same range. The common feature of these two models is the nucleation of the narrowest mounds (model 2) or islands (model 4) at the lowest temperatures; in other words, the low-temperature nucleation of high densities of mounds or islands. The temperature increase then leads to an increase in the adatom diffusion lengths that allows filling the gaps between the mounds or islands. The statistics of adatom diffusion during film growth provided a quantitative explanation of the film smoothening observed in the simulations of these models. This approach may be particularly important in the initial stages of deposition of a material on a substrate of a different material with relatively weak film-substrate interactions, in which multilayer islands are formed, because these are the most important conditions of film growth for current technologies.

Our study also considered cases of time-decreasing temperature during the deposition using the same four models. However, they are generally deleterious because the final film roughness is larger than that obtained in deposition at some constant temperature within the same range.

We also developed a method to interpolate the film roughness evolution obtained in KMC simulations at constant temperatures. Using this method, we can estimate the roughness evolution at any temperature within the simulated range, i.e., we could build an interpolated roughness function $W_I(T, \theta)$ for each growth model. We then checked whether the method would be able to predict the roughness evolution in time-varying temperature by comparing the roughness measured in the KMC simulations and $W_I(T(t), \theta(t))$.

However, the general qualitative trends of the roughness were captured by this interpolation method only in models 1 and 2, while some large quantitative deviations from direct simulation results were observed in all models. This means that the growth history in time-varying temperature cannot be predicted by the data obtained in constant temperature deposition.

ACKNOWLEDGMENTS

The authors thank Prof. Frank Schreiber for a critical reading of the manuscript and for the suggestions to improve it.

F.D.A.A.R. acknowledges support from the Brazilian agencies CNPq (Grant No. 305570/2022-6), FAPERJ (Grants No. E-26/210.040/2020, No. E-26/201.050/2022, and No. E-26/210.629/2023), and CAPES (Grant No. 88881.700849/2022-01). E.E.M.L. acknowledges support from CNPq (Grant No. 150952/2023-6). T.A.d.A. acknowledges support from CNPq (Grant No 305688/2023-5) and from the Institute of Physics at the Federal University of Bahia, where part of this work was carried out.

E.E.M.L.: Methodology, software, visualization, validation, investigation, formal analysis, and data curation.

T.A.D.A.: Methodology, investigation, formal analysis, visualization, validation, and funding acquisition.

F.D.A.A.R.: Writing - original draft, writing - review and editing, conceptualization, methodology, formal analysis, supervision, resources, project administration, and funding acquisition.

DATA AVAILABILITY

The data that support the findings of this article are openly available [58].

[1] M. Ohring, *Materials Science of Thin Films - Deposition and Structure*, 2nd ed. (Academic Press, New York, USA, 2001)

[2] N. Klipfel, A. O. Alvarez, H. Kanda, A. A. Sutanto, C. Igci, C. Roldán-Carmona, C. Momblona, F. Fabregat-Santiago, and M. K. Nazeeruddin, C_60 thin films in perovskite solar cells: Efficient or limiting charge transport layer? ACS Appl. Energy Mater. **5**, 1646 (2022).

[3] K. Qiao, $C_6$0-modified reduced-graphene-oxide-based p-type vertical organic field-effect transistors for future complementary circuits, ACS Appl. Nano Mater. **6**, 18446 (2023).

[4] M. Siegert and M. Plischke, Slope selection and coarsening in molecular beam epitaxy, Phys. Rev. Lett. **73**, 1517 (1994).

[5] J. A. Stroscio, D. T. Pierce, M. D. Stiles, A. Zangwill, and L. M. Sander, coarsening of unstable surface features during Fe(001) homoepitaxy, Phys. Rev. Lett. **75**, 4246 (1995).

[6] M. C. Bartelt and J. W. Evans, Transition to multilayer kinetic roughening for metal (100) homoepitaxy, Phys. Rev. Lett. **75**, 4250 (1995).

[7] L. Tang, P. Smilauer, and D. Vvedensky, Noise-assisted mound coarsening in epitaxial growth, Eur. Phys. J. B **2**, 409 (1998).

[8] T. Michely and J. Krug, *Islands, Mounds, and Atoms* (Springer, 2003).

[9] A. Pimpinelli and J. Villain, *Physics of Crystal Growth* (Cambridge University Press, 1998).

[10] J. W. Evans, P. A. Thiel, and M. C. Bartelt, Morphological evolution during epitaxial thin film growth: Formation of 2D islands and 3D mounds, Surf. Sci. Rep. **61**, 1 (2006).

[11] G. Abadias, L. Simonot, J. J. Colin, A. Michel, S. Camelio, and D. Babonneau, Volmer-Weber growth stages of polycrystalline metal films probed by *in situ* and real-time optical diagnostics, Appl. Phys. Lett. **107**, 183105 (2015).

[12] Y. Liu, T. Zhou, M. Sun, D. Zhao, Q. Wei, Y. Sun, R. Wang, F. Jin, Q. Niu, and Z. Su, Scaling behavior and morphology evolution of $CH_3NH_3PbI_3$ perovskite thin films grown by thermal evaporation, Mater. Res. Express **4**, 075510 (2017).

[13] S. Parveen, S. Obaidulla, and P. K. Giri, Growth kinetics of hybrid perovskite thin films on different substrates at elevated temperature and its direct correlation with the microstructure and optical properties, Appl. Surf. Sci. **530**, 147224 (2020).

[14] T. B. T. To, R. Almeida, S. O. Ferreira, and F. D. A. Aarão Reis, Roughness and correlations in the transition from island to film growth: Simulations and application to CdTe deposition, Appl. Surf. Sci. **560**, 149946 (2021).

[15] B. Reisz, E. Empting, M. Zwadlo, M. Hodas, G. Duva, V. Belova, C. Zeiser, J. Hagenlocher, S. Maiti, A. Hinderhofer, A. Gerlach, M. Oettel, and F. Schreiber, Thin film growth of phase-separating phthalocyanine-fullerene blends: A combined experimental and computational study, Phys. Rev. Mater. **5**, 045601 (2021).

[16] D. Lapkin, I. S. S. Carrasco, C. C. Luukkonen, O. Konovalov, A. Hinderhofer, F. Schreiber, F. D. A. A. Reis, and M. Oettel, Nonmonotonic roughness evolution in film growth on weakly interacting substrates, Phys. Rev. Lett. **136**, 076202 (2026).

[17] E. Empting, M. Klopotek, A. Hinderhofer, F. Schreiber, and M. Oettel, Lattice gas study of thin-film growth scenarios and transitions between them: Role of substrate, Phys. Rev. E **103**, 023302 (2021).

[18] F. Munko, C. Cruz Luukkonen, I. S. S. Carrasco, F. D. A. Aarão Reis, and M. Oettel, Island formation in heteroepitaxial growth, Phys. Rev. E **111**, 035501 (2025).

[19] A. Barabási and H. E. Stanley, *Fractal Concepts in Surface Growth* (Cambridge University Press, New York, USA, 1995).

[20] J. Krug, Origins of scale invariance in growth processes, Adv. Phys. **46**, 139 (1997).

[21] T. A. de Assis and F. D. A. Aarão Reis, Thin film deposition with time-varying temperature, J. Stat. Mech. P10008 (2013).

[22] Y. Shapir, S. Raychaudhuri, D. G. Foster, and J. Jorne, Scaling behavior of cyclical surface growth, Phys. Rev. Lett. **84**, 3029 (2000).

[23] M. Pradas, J. M. López, and A. Hernández-Machado, Time-dependent couplings and crossover length scales in nonequilibrium surface roughening, Phys. Rev. E **76**, 010102(R) (2007).

[24] Y.-L. Chou and M. Pleimling, Parameter-free scaling relation for nonequilibrium growth processes, Phys. Rev. E **79**, 051605 (2009).

[25] Y. Chou and M. Pleimling, Characterization of non-equilibrium growth through global two-time quantities, J. Stat. Mech. (2010) P08007.

[26] T. A. de Assis and F. D. A. A. Reis, Relaxation after a change in the interface growth dynamics, Phys. Rev. E **89**, 062405 (2014).
[27] S. Clarke and D. D. Vvedensky, Growth kinetics and step density in reflection high-energy electron diffraction during molecular-beam epitaxy, J. Appl. Phys. **63**, 2272 (1988).
[28] G. Ehrlich and F. G. Hudda, Atomic view of surface self-diffusion: Tungsten on tungsten, J. Chem. Phys. **44**, 1039 (1966).
[29] R. L. Schwöebel, Step motion on crystal surfaces. II, J. Appl. Phys. **40**, 614 (1969).
[30] J. Villain, Continuum models of crystal growth from atomic beams with and without desorption, J. Phys. I France **1**, 19 (1991).
[31] Z.-W. Lai and S. Das Sarma, Kinetic growth with surface relaxation: Continuum versus atomistic models, Phys. Rev. Lett. **66**, 2348 (1991).
[32] J. W. Evans, D. E. Sanders, P. A. Thiel, and A. E. DePristo, Low-temperature epitaxial growth of thin metal films, Phys. Rev. B **41**, 5410 (1990).
[33] H. C. Kang and J. W. Evans, Scaling analysis of surface roughness and Bragg oscillation decay in models for low-temperature epitaxial growth, Surf. Sci. **271**, 321 (1992).
[34] J. G. Amar and F. Family, Effects of crystalline microstructure on epitaxial growth, Phys. Rev. B **54**, 14742 (1996).
[35] M. Siegert and M. Plischke, Formation of pyramids and mounds in molecular beam epitaxy, Phys. Rev. E **53**, 307 (1996).
[36] J. G. Amar, Mechanisms of mound coarsening in unstable epitaxial growth, Phys. Rev. B **60**, R11317(R) (1999).
[37] M. C. Bartelt and J. W. Evans, Temperature dependence of kinetic roughening during metal(100) homoepitaxy: Transition between 'mounding' and smooth growth, Surf. Sci. **423**, 189 (1999).
[38] D. Moldovan and L. Golubovic, Interfacial coarsening dynamics in epitaxial growth with slope selection, Phys. Rev. E **61**, 6190 (2000).
[39] J. P. Schneider, D. Margetis, F. Gibou, and C. Ratsch, An examination of scaling behavior in unstable epitaxial mound growth via kinetic Monte Carlo simulations, J. Phys.: Condens. Matter **31**, 365301 (2019).
[40] J. Wollschläger and M. I. Larsson, Step barrier effects during early stages of the kinetic roughening of fcc(111) surfaces, J. Vac. Sci. Technol. A **40**, 013210 (2022).
[41] I. S. S. Carrasco, T. B. T. To, and F. D. A. Aarão Reis, Scaling of surface roughness in film deposition with height-dependent step edge barriers, Phys. Rev. E **108**, 064802 (2023).
[42] E. E. M. Luis, I. S. S. Carrasco, and F. D. A. Aarão Reis, Layer-by-layer growth, apparent instability, and mound coarsening in thin film deposition controlled by thermally activated surface diffusion, Mater. Today Commun. **42**, 111122 (2025).
[43] C. Ratsch, P. Smilauer, A. Zangwill, and D. D. Vvedensky, Submonolayer epitaxy without a critical nucleus, Surf. Sci. **329**, L599 (1995).
[44] C. Zhang, M. C. Bartelt, J. Wen, C. J. Jenks, J. W. Evans, and P. A. Thiel, Submonolayer island formation and the onset of multilayer growth during Ag/Ag(100) homoepitaxy, Surf. Sci. **406**, 178 (1998).
[45] T. A. de Assis and F. D. A. Aarão Reis, Dynamic scaling and temperature effects in thin film roughening, J. Stat. Mech. **2015**, P06023 (2015).
[46] X. N. Zhang, E. Barrena, D. Goswami, D. G. de Oteyza, C. Weis, and H. Dosch, Evidence for a layer-dependent Ehrlich-Schwöbel barrier in organic thin film growth, Phys. Rev. Lett. **103**, 136101 (2009).
[47] G. Hlawacek, P. Puschnig, P. Frank, A. Winkler, C. Ambrosch-Draxl, and C. Teichert, Characterization of step-edge barriers in organic thin-film growth, Science **321**, 108 (2008).
[48] R. Ganapathy, M. R. Buckley, S. J. Gerbode, and I. Cohen, Direct Measurements of island growth and step-edge barriers in colloidal epitaxy, Science **327**, 445 (2010).
[49] S. Bommel, N. Kleppmann, C. Weber, H. Spranger, P. Schäfer, J. Novak, S. V. Roth, F. Schreiber, S. H. L. Klapp, and S. Kowarik, Unravelling the multilayer growth of the fullerene C_{60} in real time, Nat. Commun. **5**, 5388 (2014).
[50] J. A. Creeden, S. E. Madaras, D. B. Beringer, I. Novikova, and R. A. Lukaszew, Intrinsic anomalous scaling of epitaxial vanadium dioxide thin films on titanium dioxide, AIP Adv. **9**, 095045 (2019).
[51] S. Rondiya, A. Rokade, A. Funde, M. Kartha, H. Pathan, and S. Jadkar, Synthesis of CDS thin films at room temperature by RF-magnetron sputtering and study of its structural, electrical, optical and morphology properties, Thin Solid Films **631**, 41 (2017).
[52] F. F. Leal, S. C. Ferreira, and S. O. Ferreira, Modelling of epitaxial film growth with an Ehrlich–Schwoebel barrier dependent on the step height, J. Phys.: Condens. Matter **23**, 292201 (2011).
[53] I. S. S. Carrasco and T. J. Oliveira, Universality and dependence on initial conditions in the class of the nonlinear molecular beam epitaxy equation, Phys. Rev. E **94**, 050801(R) (2016).
[54] T. B. T. To and F. D. A. Aarão Reis, Temperature effects in the initial stages of heteroepitaxial film growth, Surfaces **5**, 251 (2022).
[55] F. D. A. Aarão Reis, Dynamic scaling in thin-film growth with irreversible step-edge attachment, Phys. Rev. E **81**, 041605 (2010).
[56] See Supplemental Material at http://link.aps.org/supplemental/10.1103/2hd9-tfbb for additional roughness plots and views of the deposits.
[57] E. E. Mozo Luis, I. S. S. Carrasco, T. A. de Assis, and F. D. A. Aarão Reis, Statistics of adatom diffusion in a model of thin film growth, Phys. Rev. E **102**, 012805 (2020).
[58] https://github.com/Mozo55/VaryingTemperature.git.